Copper Substrate Electrode for Efficient Top-illuminated Organic Photovoltaics

H. Jessica Pereira[1] and Ross A. Hatton[1]*

[1] H. Jessica Pereira and Dr. R. A. Hatton

Department of Chemistry,

University of Warwick,

CV4 7AL, Coventry, United Kingdom

E-mail: (Ross.Hatton@warwick.ac.uk)

Abstract

It is now recognized that for solution processed organic photovoltaics (OPVs) to be manufactured on a large scale the thickness of the photoactive layer must be substantially increased beyond the currently used ≤150 nm. We show that copper can replace silver as the reflective substrate electrode in high performance top-illuminated OPVs without compromising device power conversion efficiency when the photoactive layer is thick enough to absorb the majority of incident photons on first pass through the photo-active layer. Copper is one hundredth of the cost of Ag, enabling a significant reduction in the bill of materials for OPV manufacture.

Keywords: copper, copper electrode, top illuminated, organic photovoltaic, thick bulk-heterojunction

Organic Photovoltaic (OPV) devices have recently achieved a record power conversion efficiency of 17.3%[1] using solution processed bulk-heterojunction (BHJ) light harvesting layers and so have reached the efficiency needed for a broad range of emerging applications.[2,3] Key advantages of OPVs over other thin film PVs, are their compatibility with high-speed roll-to-roll processing and that rare or toxic elements can be completely avoided, which minimises materials cost[4] and ensures environmental sustainability. Many different OPV device architectures have been developed falling into the categories of conventional, inverted, top-illuminated, semi-transparent and multi-junction, each offering advantages for particular applications or fabrication methods. For OPVs based on a single BHJ layer, conventional wisdom dictates that the power conversion efficiency is maximised when one of the electrodes is highly reflective across the full range of wavelengths over which the BHJ absorbs, because the thickness of the BHJ in most efficient single junction OPVs reported to date is only 100-150 nm which is insufficient to absorb all of the incident light across all wavelengths on the first pass through the BHJ layer. This constraint on the thickness of the light harvesting layer stems from the low and mismatched charge carrier mobility in the donor and acceptor phases comprising the BHJ.[5,6] In recent years there has been a concerted effort towards developing solution processed OPVs with high performance using a much thicker BHJ of up to 400 nm,[7–9] because it is now clear that the high defect density associated with much thinner BHJ layers together with the difficulty in achieving a uniform layer thickness over large areas using low cost printing methods when the BHJ is very thin, are serious obstacles to large scale manufacture.[6,10–13] Whilst there are relatively few BHJs suitable for thicker junction OPVs, this paradigm is beginning to shift since it is now understood that if the charge carrier mobility in the donor and acceptor phases are sufficiently high and well matched it is possible to increase the junction thickness[6,12] to ~ 400 nm without incurring an unacceptable increase in device series resistance.[6–9,12] At the same time, for many applications the top-illuminated device architecture, in which the substrate electrode is the opaque electrode and light enters the device through the transparent top electrode,[14] is particularly attractive for a wide range of applications including in automotive[15] and buildings integration[16] applications.

Using an opaque bottom electrode has the advantage that it enables much more flexibility in the choice of substrate by removing the need to use conducting oxide coated glass or plastic.[17] Whilst there have been continuous developments in the materials used for top-illuminated OPVs with regard to device engineering[18–20], the substrate electrode used is invariably silver (Ag) because it is highly reflective in the wavelength range of 350 – 900 nm and offers good stability towards oxidation in air.[18,20] However, using a Ag layer that is sufficiently thick to be optically opaque (> 80 nm) as the reflective electrode seriously erodes the cost advantage of OPVs,[21] since Ag is a high cost metal. Consequently, there is a need to identify a viable much lower cost alternative to Ag for this important class of OPVs. Copper (Cu) is an attractive replacement for Ag in this context because it is less than 1% of the cost of Ag with comparable electrical conductivity.[22] However to date there are no reports of using Cu as the reflective substrate electrode in top-illuminated OPVs presumably because the reflectance of Cu for wavelengths < 600 nm is less than 60% of that of Ag due to absorptive losses associated with inter-band transitions,[22,23] which renders it unsuitable for OPVs with a light harvesting layer ≤150 nm. Additionally, Cu is more susceptible to air oxidation than Ag, limiting the extent to which Cu electrodes can be manipulated in air prior to device fabrication, and arguably also limiting the long-term device stability, since slow air ingress into the device is inevitable. Addressing the latter issue, we have recently shown that Cu can be passivated towards oxidation in air without electrical isolation or significantly altering the optical properties, rendering it as stable as Ag.[24]

Herein we show, using the model BHJ; PCE10 (poly[4,8-bis(5-(2-ethylhexyl) thiophen-2-yl)benzo[1,2-b;4,5-b']dithiophene-2,6-diyl-alt-(4-(2-ethylhexyl)-3-fluorothieno[3,4-b]thiophene-)-2-carboxylate-2-6-diyl)]) and $PC_{70}BM$ ([6,6]-phenyl-C_{71}-butyric acid methyl ester), that Cu can be used as a drop-in replacement for Ag as the reflective substrate electrode in top-illuminated OPVs, without compromising device power conversion efficiency when the thickness of the BHJ is sufficient to absorb most of the incident photons with energy greater than the optical band gap of the light harvesting layer on the first pass, since Cu is as reflective as Ag at the band edge ($\lambda > 700$ nm) which in the most critical region for high performance BHJ devices.

Optically thick metal films (85 nm) were deposited onto glass substrates modified with a monolayer of 3-mercaptopropyltrimethoxysilane (MPTMS) for Ag, and a mixed monolayer of MPTMS and 3-aminopropyltrimethoxysilane (APTMS) for Cu. These molecular adhesive layers ensure that the metal films are smooth and compact by nucleating slab-like film growth at very low thickness, which helps to ensure that parasitic losses due to surface plasmon excitation[23] are minimised. A solution processed ZnO layer[25] deposited directly onto the metal substrate electrode was used as the electron-transport layer (ETL). A PCE10/$PC_{70}BM$ BHJ was employed as the photo-active material for this study because PCE10 and $PC_{70}BM$ have well-matched electron and hole mobility enabling study of BHJ thickness up to 400 nm.[26] A 10 nm molybdenum oxide hole-transport layer was deposited by thermal evaporation followed by an 11 nm thick Ag top window electrode.

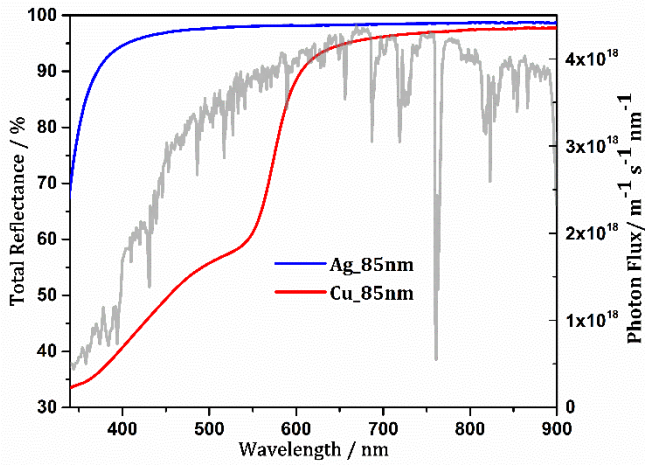

Figure 1: Total reflectance (specular and diffuse) of 85 nm thick Ag and Cu electrodes deposited by vacuum evaporation onto glass substrates derivatized with a silane molecular adhesive layer together with the AM 1.5G solar photon flux spectrum overlaid in the background.[27]

In the first instance inverted OPVs were fabricated using the previously reported optimal thickness for PCE10/$PC_{70}BM$ heterojunctions of ~100 nm.[28] In such a thin BHJ the light distribution across the photoactive layer is strongly determined by interference between the incoming light and

that reflected from the back electrode, and charge carriers are generated within the bulk of the photo-active layer regardless of the incident photon energy.[10] It is evident from Figure 1 that the reflectance of the Cu electrode is much lower than that of Ag for $\lambda \leq 600$ nm, falling to less than 60% for wavelengths below 550 nm, which at first glance would be expected to result in a significantly reduced short-circuit current density (J_{sc}) compared to identical devices using Ag as the reflective substrate electrode. However, it is important to recognize that the solar photon flux drops away steeply for $\lambda < 500$ nm (Figure 1), which moderates the adverse impact of the lower reflectivity of Cu in this region. It is also apparent from the *JV* characteristics given in Figure 2(c) that the change in J_{sc} when Cu is used in place of Ag is relatively small and there is no significant change in open-circuit voltage (V_{oc}) or device fill factor (*FF*). The external quantum efficiency (EQE) for devices using Cu as the substrate electrode (Figure 2 (d)) is lower than for devices using Ag for wavelengths < 600 nm but converges for wavelengths ≥ 650 nm, and in both cases the EQE is highest for wavelengths > 600 nm, which is qualitatively consistent with the difference in the reflectance of the Cu and Ag substrate electrodes weighted by the solar photon flux. Simulation of the optical field distribution using transfer matrix model with extinction coefficient (k) = 0 for the BHJ (Figure 2(a) & (b)), show that there is a cavity resonance condition at $\lambda \sim 700$ nm, and so photons with wavelength at and near to this value make a disproportionate contribution to J_{sc} as is evident from the EQE. Consequently, because of this strong optical interference effect, the average power conversion efficiency when Cu is used as the substrate electrode is only fractionally lower than when Ag is used (5.56% and 5.79% respectively (Table 1)).

Bottom Electrode	**Active Layer Thickness/ nm**	**J_{sc} ± 1SD / mA cm^{-2}**	**V_{oc} ± 1SD / V**	***FF* ± 1SD**	**%PCE ± 1SD**
Cu	100	11.06 ± 0.24	0.76 ± 0.02	0.66 ± 0.01	5.56 ± 0.23
	300	10.62 ± 0.11	0.74 ± 0.01	0.60 ± 0.01	4.68 ± 0.18
	400	10.68 ± 0.21	0.74 ± 0.01	0.54 ± 0.01	4.32 ± 0.16
Ag	100	11.97 ± 0.44	0.75 ± 0.02	0.64 ± 0.01	5.79 ± 0.32
	300	10.53 ± 0.07	0.74 ± 0.01	0.59 ± 0.01	4.61 ± 0.10
	400	10.84 ± 0.22	0.74 ± 0.01	0.52 ± 0.01	4.18 ± 0.15

Table 1: Summary of current density - voltage characteristics of devices with the architecture; Cu or Ag (85 nm) / ZnO (25 nm) / PCE10 – $PC_{70}BM$ (X nm) / MoO_x (10 nm)/ Ag (11 nm); where X = 100 - 400 nm, tested under 1 sun simulated solar illumination (100 mW cm^{-2}; AM 1.5G). The error bars represent ± 1 standard deviation (± 1SD) determined from the performance of 20 - 30 devices with identical architecture.

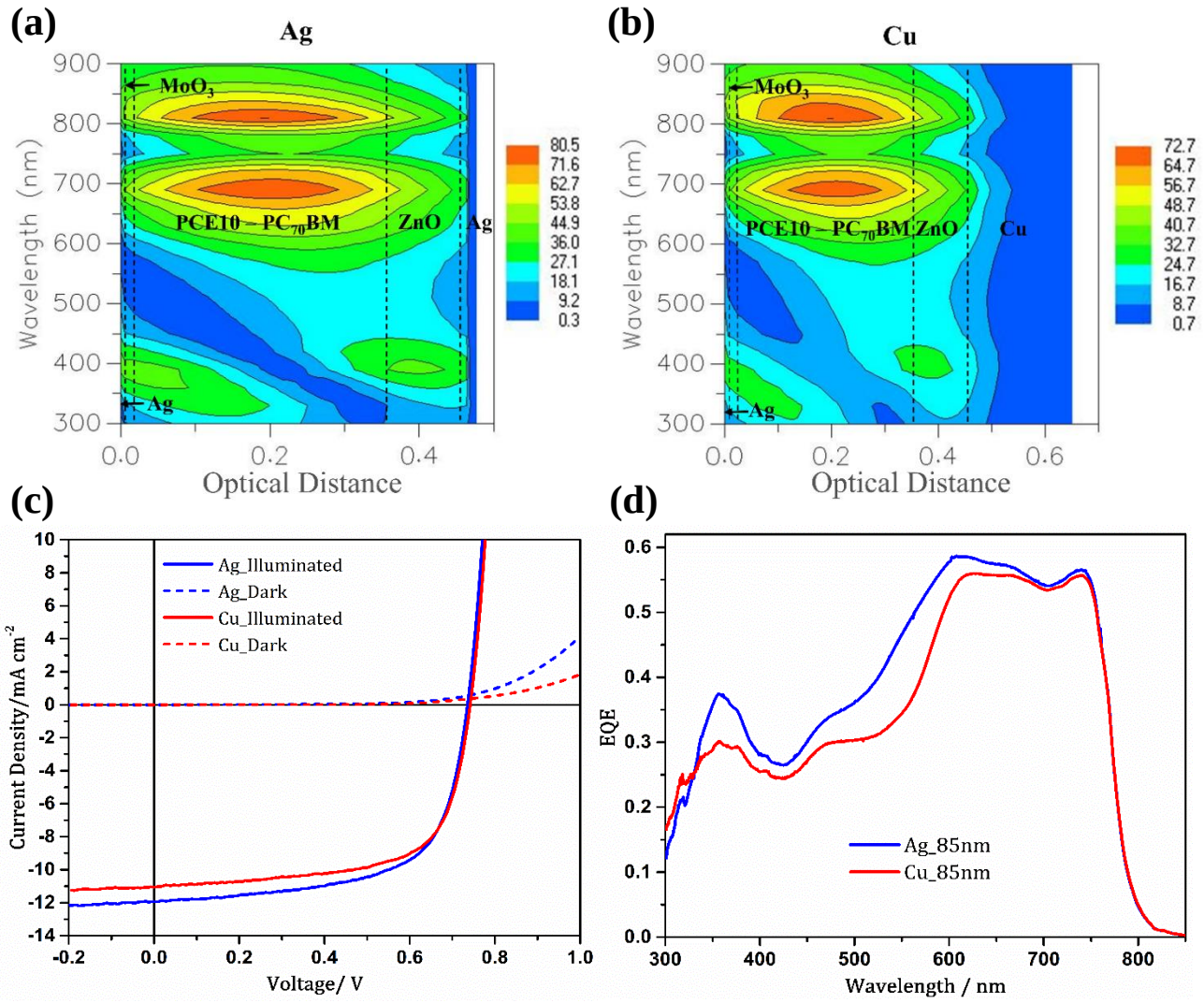

Figure 2: Simulated optical field variation for OPV devices at different wavelengths with k = 0 for the BHJ when **(a)** Ag and **(b)** Cu are used as reflective substrate electrodes. Representative **(c)** current density - voltage (*JV*) characteristics and **(d)** EQE under one sun simulated solar illumination (100 mW cm^{-2}; AM 1.5G) for devices with the architecture: Cu or Ag (85 nm) / ZnO (25 nm) / PCE10 – $PC_{70}BM$ (100 nm) / MoO_x (10 nm)/ Ag (11 nm).

For these devices, the thickness of the photoactive layer was ~ 100 nm and so over the wavelength range of 400 – 700 nm nearly 50% of the incident light is not absorbed on first pass through the BHJ layer: Figure 3(a). Consequently, the absorption of this residual light strongly depends on the efficient reflectance from the bottom substrate electrode, which directs the unabsorbed light back through the photo-active layer. Increasing the thickness of the photoactive layer increases the total amount of light absorbed on the first pass through the BHJ and when the thickness is increased to 400 nm the average absorbed light between 400 - 700 nm is increased to ~ 80%. Simulations of the optical intensity with $k = 0$ for the BHJ, show that for these thicker layers there are several cavity resonant modes occurring at ~450 nm, ~680 nm and ~820 nm for a 300 nm thick BHJ and at ~425nm, ~575nm and ~750 nm for the 400 nm thick BHJ (Figures S1 and S2). However, in the limit where all of the incident light is absorbed on first pass through the BHJ only the cavity resonance effect at the optical edge is of importance for photocurrent generation, since for shorter wavelengths there is a Beer-Lambert like optical field distribution (Figure S1 and S2). It is evident from (Figure 3(b) - (e)) that with increasing BHJ layer thickness, the J_{sc} and shape of the EQE spectrum when Ag and Cu are used as substrate electrodes converge, such that they are essentially identical when the BHJ is 400 nm in thickness. Increasing the thickness from 300 nm to 400 nm also shifts the cavity resonance so that it is more closely matched to the absorption edge: Figure S1 & S2, which is a significant advantage since it helps to extend the light harvesting capability of the device by a further ~50 nm as evidenced by Figure 3(d) & (e).

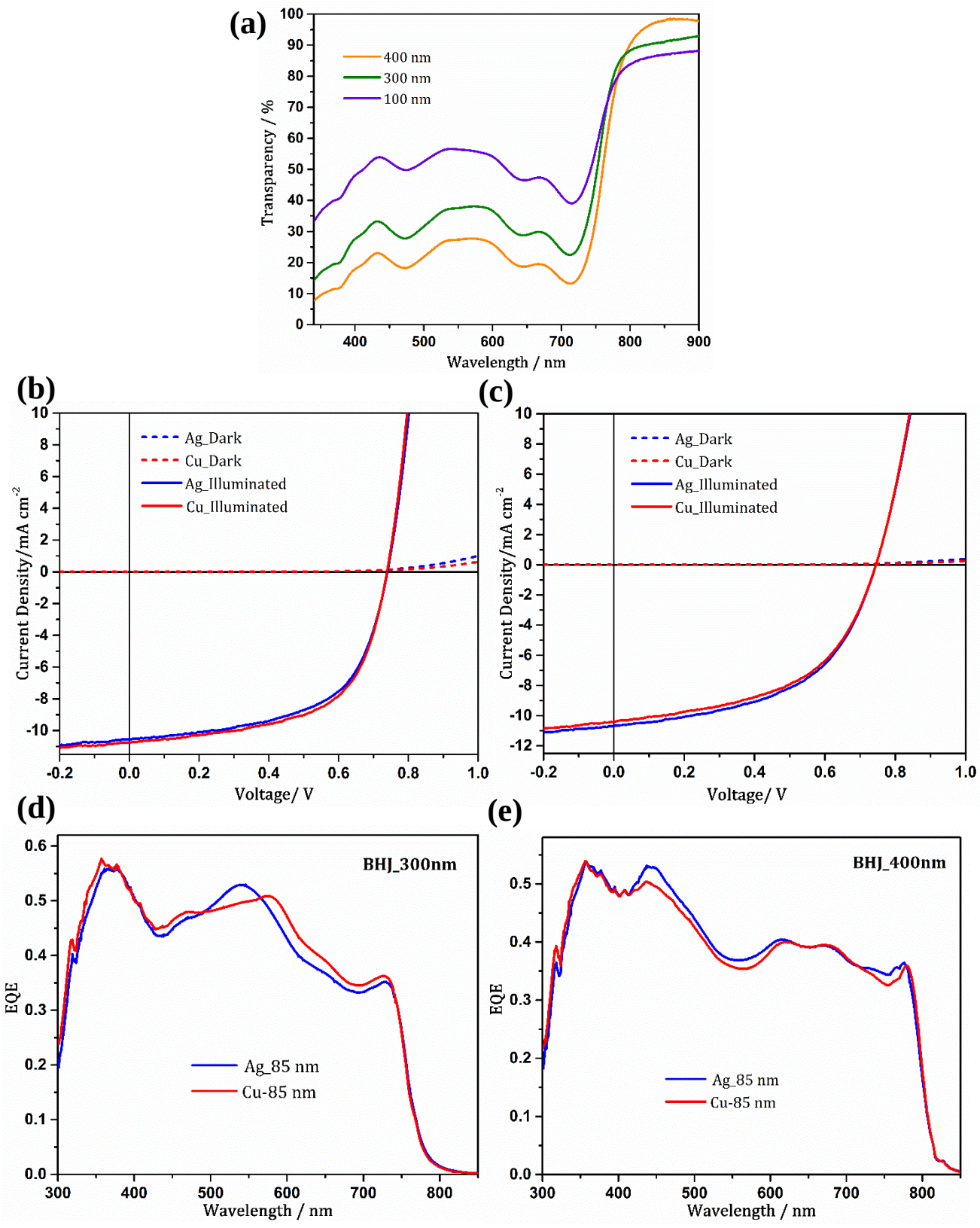

Figure 3: (a) Transmittance of the PCE10 – $PC_{70}BM$ BHJ at different thicknesses; representative current density – voltage characteristics for devices with the architecture: Cu or Ag (85 nm) / ZnO (25 nm) / PCE10 – $PC_{70}BM$ (X nm) / MoO_x (10 nm)/ Ag (11 nm) measure under one sun simulated

solar illumination (100 mW cm^{-2}; AM 1.5G) where **(b)** X = 300 nm and **(c)** X = 400 nm; **(d)** and **(e)** are representative EQE for devices given in (b) and (c) respectively.

Interestingly, in Figures 2 and 3 the onset of forward current injection in the dark is greatly suppressed as compared to that under illumination, which is atypical for OPVs. The large disparity in current density in the dark and light for $V > V_{oc}$ disappears after a few minutes of constant illumination, although is restored when the device is kept in the dark for an extended period: Figure S3. When the ZnO layer is substituted with a very thin (0.8 nm) aluminium layer[24] (which also enables efficient extraction of electrons)[29] this anomaly in the dark current characteristic does not occur; Figure S4, indicating that it is associated with the use of a ZnO electron extraction layer.[30] This behaviour has previously been reported for OPVs using a ZnO electron extraction layer[30] and is attributed to UV light induced O_2 desorption from the ZnO, followed by its re-adsorption in the dark.

Notably, the power conversion efficiency of the model top-illuminated devices used in this study is lower than that achievable using indium-tin oxide (ITO) glass as the transparent electrode, because the semi-transparent top Ag (11 nm) electrode reflects ~ 36% of the incident light before it can enter the BHJ layer (Supporting Information S5 and S6). It is expected that optimisation of the transparency of the top electrode, either by using a thinner Ag top-electrode and/or Ag grid in conjunction with an anti-reflecting layer, would reduce the reflectance to < 10%, such that substantially more light could be coupled into the device.

Conclusion

In summary we have shown that optically thick Cu films can be used as a drop-in replacement for reflective Ag electrodes in efficient top-illuminated OPV devices without sacrificing device efficiency, when the photo-active layer is thick enough to absorb most of the incident light on first pass through the BHJ layer, since Cu is as reflective as Ag where it matters most for high performance BHJ devices; i.e. at the band edge ($\lambda > 700$ nm). Given the inevitable transition to BHJs with a thickness of ≥ 300 nm in the coming years, using Cu in place of Ag will ensure that the bill of materials for the reflective substrate electrode is a small part of the total device cost.

Supporting Information

All data supporting this study are provided as supplementary information accompanying this paper.

Figure S1: Transfer matrix simulation of the optical field in OPV devices with the structure: reflective substrate electrode / ZnO (25 nm) / PCE10 – $PC_{70}BM$ (300 nm) / MoO_x (10 nm)/ Ag (11 nm); Figure S2: Transfer matrix simulation of the optical field in OPV devices with the structure: reflective substrate electrode / ZnO (25 nm) / PCE10 – $PC_{70}BM$ (400 nm) / MoO_x (10 nm)/ Ag (11 nm); Figure S3: Representative dark current density – voltage characteristics for a top-illuminated OPV device with the architecture: Cu (85 nm) / ZnO (25 nm) / PCE10 – $PC_{70}BM$ (100 nm) / MoO_x (10 nm)/ Ag (11 nm) measured after different periods under one sun simulated solar illumination (100 mW cm^{-2}; AM 1.5G); Figure S4: Representative current density – voltage characteristics for top-illuminated OPV devices with the architecture: Cu (85 nm) / Al (0.8 nm) / PCE10 – $PC_{70}BM$ (100 nm) / MoO_x (10 nm)/ Ag (11 nm) measured under one sun simulated solar illumination (100 mW cm^{-2}; AM 1.5G); Figure S5: Transfer matrix simulation of the reflectance from the top 11 nm Ag electrode in a top-illuminated OPV with the architecture: Ag (85nm) / ZnO (25 nm) / PCE10 – $PC_{70}BM$ (300 nm) / MoOx (10 nm)/ Ag (11 nm); Figure S6: Transfer matrix simulation of the reflectance from the ITO

glass electrode in an OPV with the architecture: Ag (85nm) / ZnO (25 nm) / PCE10 – $PC_{70}BM$ (300 nm) / MoOx (10 nm)/ ITO glass and experimental methods.

Acknowledgements

The authors would like to thank the United Kingdom Engineering and Physical Sciences Research Council (EPSRC) for funding (Grant number: EP/N009096/1) and the University of Warwick for the award of a Chancellor's International Scholarship to H. Jessica Pereira.

References

(1) Meng, L.; Zhang, Y.; Wan, X.; Li, C.; Zhang, X.; Wang, Y.; Ke, X.; Xiao, Z.; Ding, L.; Xia, R.; Yip, H.; Cao, Y.; Chen, Y. Organic and Solution-Processed Tandem Solar Cells with 17.3% Efficiency. *Science* **2018**, *361* (6407), 1094–1098.

(2) Wong, W. S.; Salleo, A. *Flexible Electronics : Materials and Applications*; Springer, 2008.

(3) Zamarayeva, A. M.; Ostfeld, A. E.; Wang, M.; Duey, J. K.; Deckman, I.; Lechene, B. P.; Davies, G.; Steingart, D. A.; Arias, A. C. Flexible and Stretchable Power Sources for Wearable Electronics. *Sci Adv* **2017**, *3* (6), e1602051.

(4) Wöhrle, D.; Meissner, D.; Wohrle, B. D.; Meissner, D. Organic Solar Cells. *Adv. Mater.* **1991**, *3* (3), 129–138.

(5) Chen, L.-M.; Xu, Z.; Hong, Z.; Yang, Y. Interface Investigation and Engineering – Achieving High Performance Polymer Photovoltaic Devices. *J. Mater. Chem.* **2010**, *20* (13), 2575–2598.

(6) Armin, A.; Hambsch, M.; Wolfer, P.; Jin, H.; Li, J.; Shi, Z.; Burn, P. L.; Meredith, P. Efficient, Large Area, and Thick Junction Polymer Solar Cells with Balanced Mobilities and

Low Defect Densities. *Adv. Energy Mater.* **2015**, *5* (3), 1401221.

(7) Sun, C.; Pan, F.; Bin, H.; Zhang, J.; Xue, L.; Qiu, B.; Wei, Z.; Zhang, Z. G.; Li, Y. A Low Cost and High Performance Polymer Donor Material for Polymer Solar Cells. *Nat. Commun.* **2018**, *9* (1), 1–10.

(8) Liu, X.; Ye, L.; Zhao, W.; Zhang, S.; Li, S.; Su, G. M.; Wang, C.; Ade, H.; Hou, J. Morphology Control Enables Thickness-Insensitive Efficient Nonfullerene Polymer Solar Cells. *Mater. Chem. Front.* **2017**, *1*, 2057–2064.

(9) Zhang, G.; Zhang, K.; Yin, Q.; Jiang, X. F.; Wang, Z.; Xin, J.; Ma, W.; Yan, H.; Huang, F.; Cao, Y. High-Performance Ternary Organic Solar Cell Enabled by a Thick Active Layer Containing a Liquid Crystalline Small Molecule Donor. *J. Am. Chem. Soc.* **2017**, *139* (6), 2387–2395.

(10) Armin, A.; Yazmaciyan, A.; Hambsch, M.; Li, J.; Burn, P. L.; Meredith, P. Electro-Optics of Conventional and Inverted Thick Junction Organic Solar Cells. *ACS Photonics* **2015**, *2* (12), 1745–1754.

(11) Zang, Y.; Xin, Q.; Zhao, J.; Lin, J. Effect of Active Layer Thickness on the Performance of Polymer Solar Cells Based on a Highly Efficient Donor Material of PTB7-Th. *J. Phys. Chem. C* **2018**, *122* (29), 16532–16539.

(12) Moulé, A. J.; Bonekamp, J. B.; Meerholz, K. The Effect of Active Layer Thickness and Composition on the Performance of Bulk-Heterojunction Solar Cells. *J. Appl. Phys.* **2006**, *100* (9), 94503.

(13) Yang, J.; Vak, D.; Clark, N.; Subbiah, J.; Wong, W. W. H.; Jones, D. J.; Watkins, S. E.; Wilson, G. Organic Photovoltaic Modules Fabricated by an Industrial Gravure Printing Proofer. *Sol. Energy Mater. Sol. Cells* **2013**, *109*, 47–55.

(14) Jiang, Y.; Luo, B.; Jiang, F.; Jiang, F.; Fuentes-Hernandez, C.; Liu, T.; Mao, L.; Xiong, S.;

Li, Z.; Wang, T.; et al. Efficient Colorful Perovskite Solar Cells Using a Top Polymer Electrode Simultaneously as Spectrally Selective Antireflection Coating. *Nano Lett.* **2016**, *16* (12), 7829–7835.

(15) Granqvist, C. G. Transparent Conductors as Solar Energy Materials: A Panoramic Review. *Sol. Energy Mater. Sol. Cells* **2007**, *91* (17), 1529–1598.

(16) Miyazaki, T.; Akisawa, A.; Kashiwagi, T. Energy Savings of Office Buildings by the Use of Semi-Transparent Solar Cells for Windows. *Renew. Energy* **2005**.

(17) Qin, F.; Tong, J.; Ge, R.; Luo, B.; Jiang, F.; Liu, T.; Jiang, Y.; Xu, Z.; Mao, L.; Meng, W.; et al. Indium Tin Oxide (ITO)-Free, Top-Illuminated, Flexible Perovskite Solar Cells. *J. Mater. Chem. A* **2016**, *4* (36), 14017–14024.

(18) Lin, H. W.; Chiu, S. W.; Lin, L. Y.; Hung, Z. Y.; Chen, Y. H.; Lin, F.; Wong, K. T. Device Engineering for Highly Efficient Top-Illuminated Organic Solar Cells with Microcavity Structures. *Adv. Mater.* **2012**, *24* (17), 2269–2272.

(19) Zhang, C.; Zhao, D.; Gu, D.; Kim, H.; Ling, T.; Wu, Y. K. R.; Guo, L. J. An Ultrathin, Smooth, and Low-Loss Al-Doped Ag Film and Its Application as a Transparent Electrode in Organic Photovoltaics. *Adv. Mater.* **2014**.

(20) Ham, J.; Dong, W. J.; Park, J. Y.; Yoo, C. J.; Lee, I.; Lee, J. L. A Challenge beyond Bottom Cells: Top-Illuminated Flexible Organic Solar Cells with Nanostructured Dielectric/Metal/Polymer (DMP) Films. *Adv. Mater.* **2015**, *27* (27), 4027–4033.

(21) Søndergaard, R. R.; Espinosa, N.; Jørgensen, M.; Krebs, F. C. Efficient Decommissioning and Recycling of Polymer Solar Cells: Justification for Use of Silver. *Energy Environ. Sci.* **2014**, *7* (3), 1006–1012.

(22) West, P. R.; Ishii, S.; Naik, G. V.; Emani, N. K.; Shalaev, V. M.; Boltasseva, A. Searching for Better Plasmonic Materials. *Laser Photonics Rev.* **2010**, *4* (6), 795–808.

(23) Pereira, H. J.; Hutter, O. S.; Dabera, G. D. M. R.; Rochford, L. A.; Hatton, R. A. Copper Light-Catching Electrodes for Organic Photovoltaics. *Sustain. Energy Fuels* **2017**, *1* (4), 859–865.

(24) Bellchambers, P.; Lee, J.; Varagnolo, S.; Amari, H.; Walker, M.; Hatton, R. A. Elucidating the Exceptional Passivation Effect of 0.8 Nm Evaporated Aluminium on Transparent Copper Films. *Front. Mater.* **2018**, *5:71*.

(25) Pereira, H. J.; Reed, J.; Lee, J.; Varagnolo, S.; Dabera, G. D. R.; Hatton, R. A. Fabrication of Copper Window Electrodes with ≈10 8 Apertures Cm −2 for Organic Photovoltaics. *Adv. Funct. Mater.* **2018**, *28* (36), 1802893.

(26) Deshmukh, K. D.; Prasad, S. K. K.; Chandrasekaran, N.; Liu, A. C. Y.; Gann, E.; Thomsen, L.; Kabra, D.; Hodgkiss, J. M.; McNeill, C. R. Critical Role of Pendant Group Substitution on the Performance of Efficient All-Polymer Solar Cells. *Chem. Mater.* **2017**, *29* (2), 804–816.

(27) ASTM G173 - 03(2012) Standard Tables for Reference Solar Spectral Irradiances: Direct Normal and Hemispherical on 37° Tilted Surface https://www.astm.org/Standards/G173.htm (accessed Dec 6, 2018).

(28) Liao, S. H.; Jhuo, H. J.; Yeh, P. N.; Cheng, Y. S.; Li, Y. L.; Lee, Y. H.; Sharma, S.; Chen, S. A. Single Junction Inverted Polymer Solar Cell Reaching Power Conversion Efficiency 10.31% by Employing Dual-Doped Zinc Oxide Nano-Film as Cathode Interlayer. *Sci. Rep.* **2014**, *4*, 4–10.

(29) Hutter, O. S.; Stec, H. M.; Hatton, R. A. An Indium-Free Low Work Function Window Electrode for Organic Photovoltaics Which Improves with in-Situ Oxidation. *Adv. Mater.* **2013**, *25* (2), 284–288.

(30) Manor, A.; Katz, E. A.; Tromholt, T.; Krebs, F. C. Enhancing Functionality of ZnO Hole

Blocking Layer in Organic Photovoltaics. *Sol. Energy Mater. Sol. Cells* **2012**, *98*, 491–493.